LETTER

doi:10.1038/nature14670

Mutations in *DCHS1* cause mitral valve prolapse

Ronen Durst[1,2]*, Kimberly Sauls[3]*, David S. Peal[4]*, Annemarieke deVlaming[3], Katelynn Toomer[3], Maire Leyne[1], Monica Salani[1], Michael E. Talkowski[1,5], Harrison Brand[1,5], Maëlle Perrocheau[6], Charles Simpson[1], Christopher Jett[1], Matthew R. Stone[1], Florie Charles[1], Colby Chiang[1], Stacey N. Lynch[4], Nabila Bouatia-Naji[6,7], Francesca N. Delling[8], Lisa A. Freed[9], Christophe Tribouilloy[10], Thierry Le Tourneau[11], Hervé LeMarec[11], Leticia Fernandez-Friera[12,13], Jorge Solis[12,13], Daniel Trujillano[14,15,16,17], Stephan Ossowski[15,18], Xavier Estivill[14,15,16,17], Christian Dina[11,19,20,21], Patrick Bruneval[22], Adrian Chester[23], Jean-Jacques Schott[11,19,20,21], Kenneth D. Irvine[24], Yaopan Mao[24], Andy Wessels[3], Tahirali Motiwala[3], Michel Puceat[25], Yoshikazu Tsukasaki[26], Donald R. Menick[27], Harinath Kasiganesan[27], Xingju Nie[28], Ann-Marie Broome[28], Katherine Williams[3], Amanda Johnson[3], Roger R. Markwald[3], Xavier Jeunemaitre[6,7,29]§, Albert Hagege[6,7,30]§, Robert A. Levine[7,31]§, David J. Milan[1,4]§, Russell A. Norris[3]§ & Susan A. Slaugenhaupt[1]§

Mitral valve prolapse (MVP) is a common cardiac valve disease that affects nearly 1 in 40 individuals[1–3]. It can manifest as mitral regurgitation and is the leading indication for mitral valve surgery[4,5]. Despite a clear heritable component, the genetic aetiology leading to non-syndromic MVP has remained elusive. Four affected individuals from a large multigenerational family segregating non-syndromic MVP underwent capture sequencing of the linked interval on chromosome 11. We report a missense mutation in the *DCHS1* gene, the human homologue of the *Drosophila* cell polarity gene *dachsous* (*ds*), that segregates with MVP in the family. Morpholino knockdown of the zebrafish homologue *dachsous1b* resulted in a cardiac atrioventricular canal defect that could be rescued by wild-type human *DCHS1*, but not by *DCHS1* messenger RNA with the familial mutation. Further genetic studies identified two additional families in which a second deleterious *DCHS1* mutation segregates with MVP. Both *DCHS1* mutations reduce protein stability as demonstrated in zebrafish, cultured cells and, notably, in mitral valve interstitial cells (MVICs) obtained during mitral valve repair surgery of a proband. *Dchs1*$^{+/-}$ mice had prolapse of thickened mitral leaflets, which could be traced back to developmental errors in valve morphogenesis. *DCHS1* deficiency in MVP patient MVICs, as well as in *Dchs1*$^{+/-}$ mouse MVICs, result in altered migration and cellular patterning, supporting these processes as aetiological underpinnings for the disease. Understanding the role of *DCHS1* in mitral valve development and MVP pathogenesis holds potential for therapeutic insights for this very common disease.

In a previous study, based on specific diagnostic criteria[6–9], *MMVP2* (myxomatous mitral valve prolapse-2) was mapped to a 4.3 cM region of chromosome 11p15.4 in a family of Western European descent segregating non-syndromic mitral valve prolapse as an autosomal dominant trait with age-dependent penetrance (Fig. 1a, c)[6]. We performed tiled capture and high-throughput sequence analysis of genomic DNA from four affected individuals (Fig. 1a), identifying 4,891 single nucleotide variants (SNVs) and insertion/deletion polymorphisms in the targeted region (see Methods). After selecting rare protein-coding variants shared among all affected pedigree members, we identified three heterozygous protein-altering variants: two missense SNVs in *DCHS1*, a member of the cadherin superfamily[10], resulting in p.P197L and p.R2513H (Fig. 1b), and a single missense SNV in *APBB1*, the amyloid beta (A4) precursor protein-binding family B, member 1 gene resulting in p.R481H. Both *DCHS1* mutations, p.P197L and p.R2513H, were rare in the population (the former observed three times in 4,300 European-American individuals from the NHLBI Exome Sequencing Project and the latter never observed), and both were predicted to be protein damaging by PolyPhen-2 (ref. 11), LRT[12], and MutationTaster[13]. While the *APBB1* variant was also rare in population-based data, no cardiac phenotype was observed in *apbb1* morphant zebrafish, despite reduction of *apbb1* mRNA (Extended Data Fig. 1a, b). Additionally, *Apbb1* is not expressed in murine cardiac valves (Extended Data Fig. 2)[14], and no cardiac defects have been reported in the *Apbb1* knockout mouse[15]. This suggests that the *APBB1* variant is unlikely to be contributing to MVP in this family.

The functional effect of the *DCHS1* variants was evaluated in the zebrafish *Danio rerio*, as this model system lends itself to functional annotation of mutations implicated in human disease[16–18]. Zebrafish have two *DCHS1* homologues, *dachsous1a* and *dachsous1b*. *dachsous1b* is located in a region of *D. rerio* chromosome 10 that is syntenic to the *DCHS1* region of human chromosome 11. Knockdown of *dachsous1a* did not result in a cardiac phenotype despite reduction in mRNA levels

[1]Center for Human Genetic Research, Massachusetts General Hospital Research Institute and Department of Neurology, Harvard Medical School, 185 Cambridge Street, Boston, Massachusetts 02114 USA. [2]Cardiology Division, Hadassah Hebrew University Medical Center, POB 12000 Jerusalem, Israel. [3]Cardiovascular Developmental Biology Center, Department of Regenerative Medicine and Cell Biology, Department of Medicine, Children's Research Institute, Medical University of South Carolina, 171 Ashley Avenue, Charleston, South Carolina 29425, USA. [4]Cardiovascular Research Center, Cardiology Division, Massachusetts General Hospital, Harvard Medical School, 55 Fruit Street, Boston, Massachusetts 02114, USA. [5]Psychiatric and Neurodevelopmental Genetics Unit, Department of Psychiatry, Massachusetts General Hospital, Boston, Massachusetts 02114, USA. [6]INSERM, UMR-970, Paris Cardiovascular Research Center, 75015 Paris, France. [7]Université Paris Descartes, Sorbonne Paris Cité, Faculty of Medicine, 75006 Paris, France. [8]Department of Medicine (Cardiovascular Division), Beth Israel Deaconess Medical Center, Harvard Medical School, Boston, Massachusetts 02215, USA. [9]Yale-New Haven Hospital Heart and Vascular Center, Yale School of Medicine, 20 York Street, New Haven, Connecticut 06510, USA. [10]Department of Cardiology, University Hospital Amiens; INSERM U-1088, Jules Verne University of Picardie, 80000 Amiens, France. [11]Inserm U1087; Institut du Thorax; University Hospital, 44007 Nantes, France. [12]Centro Nacional de Investigaciones Cardiovasculares, Carlos III (CNIC), 28029 Madrid, Spain. [13]Hospital Universitario Monteprincipe, 28660 Madrid, Spain. [14]Genetic Causes of Disease Group, Centre for Genomic Regulation (CRG), 08003 Barcelona, Catalonia, Spain. [15]Universitat Pompeu Fabra (UPF), 08002 Barcelona, Catalonia, Spain. [16]Hospital del Mar Medical Research Institute (IMIM), 08003 Barcelona, Catalonia, Spain. [17]CIBER in Epidemiology and Public Health (CIBERESP), 08036 Barcelona, Catalonia, Spain. [18]Genomic and Epigenomic Variation in Disease Group, Centre for Genomic Regulation (CRG), 08003 Barcelona, Catalonia, Spain. [19]CNRS, UMR 6291, 44007 Nantes, France. [20]Université de Nantes, 44322 Nantes, France. [21]CHU Nantes, l'Institut du Thorax, Service de Cardiologie, 44093 Nantes, France. [22]Service d'Anatomie Pathologique, Hôpital Européen Georges Pompidou, 75015 Paris, France. [23]National Heart and Lung Institute, Harefield, Heart Science Centre, Imperial College London, London SW7 2AZ, UK. [24]Howard Hughes Medical Institute, Waksman Institute and Department of Molecular Biology and Biochemistry, Rutgers, the State University of New Jersey, Piscataway, New Jersey 08854, USA. [25]INSERM UMR_S910, Team physiopathology of cardiac development Aix-Marseille University, Medical School La Timone, 13885 Marseille, France. [26]Department of Cellular and Molecular Biology, University of Texas Health Science Center Northeast Tyler, Texas75708, USA. [27]Gazes Cardiac Research Institute, Division of Cardiology, Department of Medicine, Medical University of South Carolina, Charleston, South Carolina 29425, USA. [28]Department of Radiology and Radiological Sciences, Medical University of South Carolina, Charleston, South Carolina 29425, USA. [29]Assistance Publique – Hôpitaux de Paris, Département de Génétique, Hôpital Européen Georges Pompidou, 75015 Paris, France. [30]Assistance Publique – Hôpitaux de Paris, Département de Cardiologie, Hôpital Européen Georges Pompidou, 75015 Paris, France. [31]Cardiac Ultrasound Laboratory, Cardiology Division, Massachusetts General Hospital, Harvard Medical School, 55 Fruit Street, Boston, Massachusetts 02114, USA.

*These authors contributed equally to this work.

§These authors jointly supervised this work.

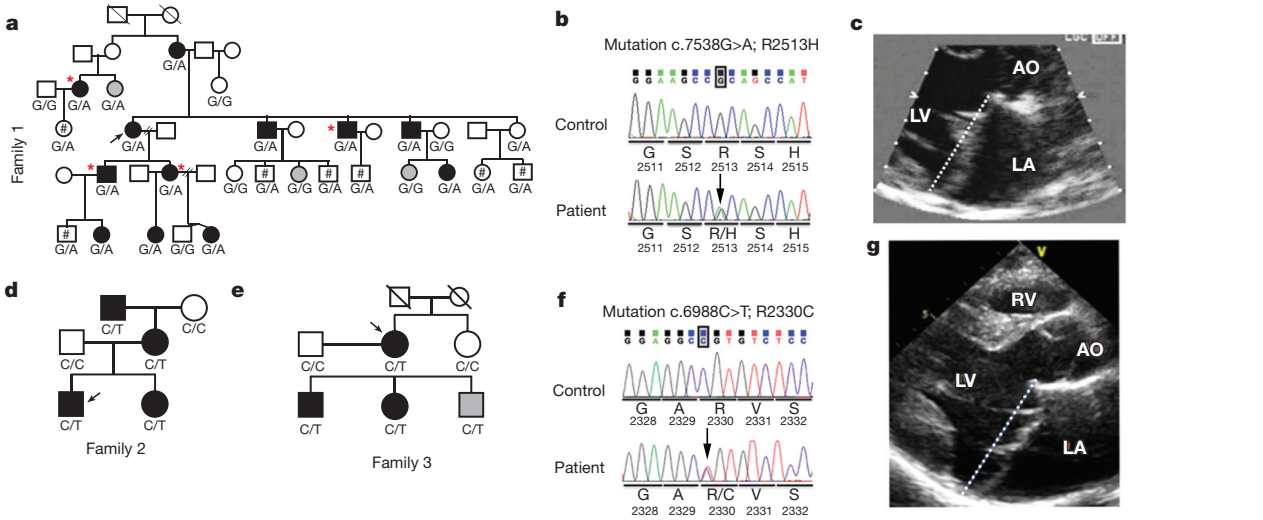

Figure 1 | Pedigrees, mutation, and phenotype. Black symbols, MVP affected, grey, unknown, arrows, probands. If no genotype is shown, the individuals were unavailable for study. **A**, Pedigree linked to chromosome 11. #, Individuals under 15 years of age; *, individuals sequenced. Genotypes c.7538G>A (R2513H) of *DCHS1* mutation are shown. **b**, DNA sequence of c.7538G>A (p.R2513H). **c**, Two-dimensional echocardiographic long-axis view of family 1 proband. Dashed line marks mitral annulus. **d**, **e**, Family 2 and 3 pedigrees. Genotype c.6988C>T (p.R2330C) shown. **f**, DNA sequence c.6988C>T (p.R2330C). **g**, Two-dimensional echocardiographic long-axis view of family 2 proband.

(Extended Data Fig. 1a, b); however, knockdown of *dachsous1b* (*dchs1b*) led to significant changes in cardiac morphology (Fig. 2a; Extended Data Fig. 1a). Control zebrafish hearts undergo looping and develop an atrioventricular constriction by 48 h post-fertilization (hpf), whereas *dchs1b* knockdown disrupts this process, resulting in impaired formation of the atrioventricular constriction (Fig. 2a, b). While control embryos have unidirectional blood flow between the atrium and ventricle at 72 hpf (Supplementary Video 4), *dchs1b* knockdown causes regurgitation of blood from the ventricle into the atrium (Supplementary Video 5). An atrioventricular canal defect was defined as failure of cardiac looping combined with any atrioventricular regurgitation at 72 hpf. Using a high morpholino dose (1.5 ng) to establish the phenotype, the prevalence of atrioventricular canal defects was 76% ($n = 170$), whereas spontaneous cardiac defects were rarely observed in controls (0.5%, $n = 205$) (Fig. 2b). Whole-mount *in situ* hybridization of *dchs1b* confirmed predominant expression at the atrioventricular junction at 54 and 72 hpf, corresponding to the temporal defects observed in the morphants (Extended Data Fig. 3a–c). We evaluated gene expression patterns in the developing atrioventricular ring, and observed that *bmp4* expression is expanded into the ventricle at 48 hpf in *dchs1b* knockdown embryos while it is restricted to the atrioventricular ring in controls (Extended Data Fig. 4a, b). Additionally, *has2* expression was not detectable at 48 hpf, and only faintly at 72 hpf in the *dchs1b* knockdown (Extended Data Fig. 4i–l). To test mutation pathogenicity in this model, rescue experiments were performed using both wild-type human *DCHS1* and P197L/R2513H mutant mRNA, which were injected into *dchs1b* knockdown zebrafish with a lower dose of morpholino (0.75 ng) to minimize combined morpholino/mRNA toxicity. Human wild-type *DCHS1* mRNA rescued the atrioventricular canal defect observed upon *dchs1b* knockdown, whereas injection of an equimolar amount of mutant *DCHS1* mRNA failed to rescue (Fig. 2c). Injection of the mutant *DCHS1* mRNA alone did not cause atrioventricular canal defects, supporting a loss-of-function mechanism for the *DCHS1* mutation.

Having demonstrated segregation of a loss-of-function *DCHS1* mutation with MVP in our large pedigree, we sought to determine if genetic variation in *DCHS1* plays a role in MVP beyond the linked family. By evaluating a cohort of MVP patients, we identified two additional families in which MVP segregated with the novel *DCHS1* protein variant p.R2330C (Fig. 1d–g). The proband of family 2 underwent surgical mitral valve repair for severe MVP and mitral

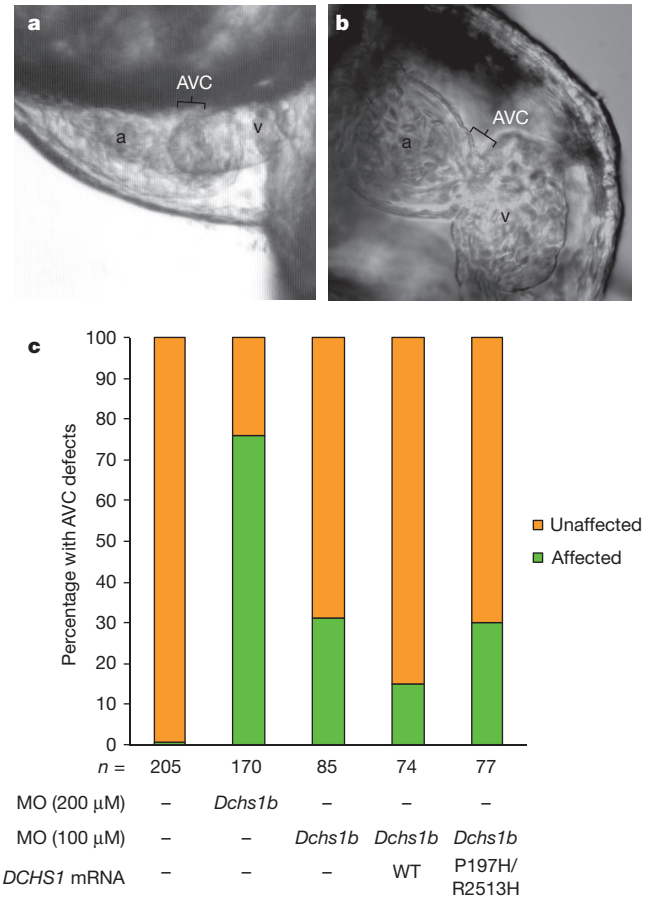

Figure 2 | Zebrafish *Dchs1b* is required for atrioventricular canal development. **a**, By 72 hpf, zebrafish hearts develop a constriction in the atrioventricular canal (AVC) that separates the atrium (a) from the ventricle (v). **b**, Knockdown of *dchs1b* results in absence of the atrioventricular constriction (bracket). **c**, Approximately 75% of *Dchs1b* morphants exhibit AVC defects ($*P = 1 \times 10^{-62}$). *DCHS1* human mRNA rescues the *dchs1b* morpholino AVC phenotype, whereas human mutant *DCHS1* mRNA (P197H/R2513H) fails to rescue the phenotype ($**P = 0.009$). The total number of fish analysed was 611 and statistical values were obtained using Fisher's exact test.

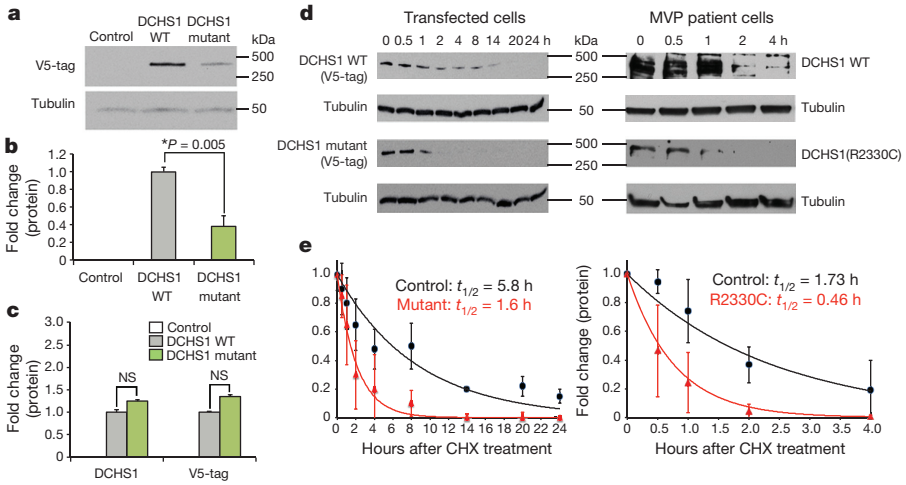

Figure 3 | *DCHS1* mutations result in diminished protein levels. **a–c**, Western blot, (p.P197L/p.R2513H) mutant *DCHS1* results in a 60% decrease in protein with no change in RNA expression. **d**, Left panel, DCHS1 wild-type (WT) or mutant (p.P197L/p.R2513H) transfectants treated with cycloheximide (CHX) for specified times followed by western blot analyses. Right panel, cycloheximide on control (DCHS1 WT) or MVP patient (p.R2330C) MVICs. Tubulin, loading control. **e**, Calculated protein half-lives. WT and mutant transfectants half-life = 5.8 h versus 1.6, respectively (left). Control and mutant *DCHS1* half-life is 1.73 h versus 0.46 h, respectively (right). Analyses performed in triplicate and repeated four times. Error bars, standard deviations; *P* values calculated using two-tailed Student's *t*-test.

regurgitation at age 21. Valve tissue was resected to repair the posterior leaflet and examination of the tissue showed classic myxomatous degeneration[19,20] (Extended Data Fig. 5). Mitral valve interstitial cells were isolated from a portion of the posterior leaflet resected during surgery, providing a unique resource for the functional studies described below. The proband's sister, evaluated at age 27 and also heterozygous for the p.R2330C mutation, demonstrated classical MVP with thickened leaflets and moderate regurgitation. The father and maternal grandmother were unaffected and do not carry the mutation. The mother (age 49) and maternal grandfather (age 76) are both affected with mild MVP and both carry p.R2330C. In family 3, the proband (Fig. 1e) had moderate to severe heart failure owing to severe mitral regurgitation with posterior leaflet prolapse requiring surgery at age 72. The proband's sister, age 69, is unaffected and negative for the p.R2330C mutation. The son (age 52) and the daughter (age 53) are both affected with MVP and both carry p.R2330C. The second son (age 55) also carries p.R2330C, however his MVP status is indeterminate due to due to mild left ventricular inferior wall hypokinesis that tethers the leaflets down into the left ventricular cavity[21], masking leaflet prolapse motion towards the left atrium.

To evaluate the functional consequence of the DCHS1 mutations, we quantified protein levels in cells transfected with either wild-type or variant (p.P197L/p.R2513H) *DCHS1* complementary DNA constructs. Expression of the *DCHS1* mutant protein was ~60% less than wild-type with no significant change in mRNA levels, suggesting that the *DCHS1* variants reduce protein stability (Fig. 3a–c). Cycloheximide treatment revealed that wild-type *DCHS1* protein in transfected cells had a half-life of 5.8 h, while the mutant *DCHS1* protein (p.P197L/p.R2513H) had a half-life of 1.6 h (Fig. 3d, e). *DCHS1* constructs harbouring either p.P197L or p.R2513H were evaluated, showing that p.R2513H markedly reduced protein levels, implicating this variant as pathogenic in the family (Fig. 1, Extended Data Fig. 6). A similar analysis of *DCHS1* protein half-life was conducted using p.R2330C MVICs from the proband of family 2. Consistent with the data obtained from the p.R2513H transfectants, these studies showed significant reduction in protein half-life compared to control MVICs ($t_{1/2}$ = 0.46 h versus 1.73 h, Fig. 3d, e). Together, our studies show that p.R2513H and p.R2330C result in *DCHS1* loss of function. In order to evaluate *DCHS1* loss of function in a mammalian model, we analysed *Dchs1*-deficient mice for phenotypic similarities to human MVP.

Homozygous knockout of *Dchs1* in mice results in neonatal lethality and multi-organ impairment[22]; however, the relevant genetic model for human MVP is the heterozygous *Dchs1* mouse. *Dchs1*$^{+/-}$ mice exhibit mitral valve prolapse with pronounced involvement of the posterior leaflet, which is elongated and shifts the leaflet coaptation anteriorly (Fig. 4) as in the proband from family 1 (Fig. 1c, Supplementary Videos 1–3, 6, 7)[23]. Micro-MRI analyses and 3D reconstructions of adult *Dchs1*$^{+/-}$ mice reveal prominent posterior leaflet

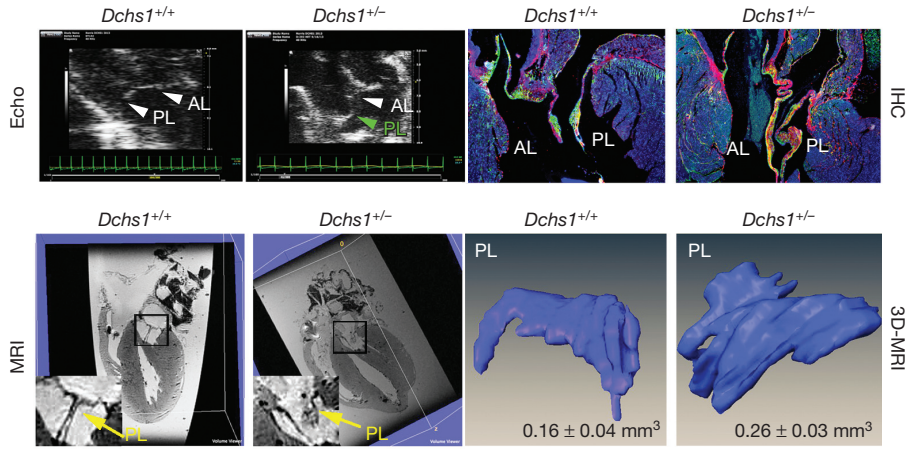

Figure 4 | *Dchs1* deficiency causes MVP and myxomatous degeneration in the adult mouse. Echocardiography (Echo), MRI, histopathology and 3D reconstructions performed on 9-month old male *Dchs1*$^{+/+}$ and *Dchs1*$^{+/-}$ mouse hearts. Echo, posterior leaflet prolapse in *Dchs1*$^{+/-}$ (green arrow) (n = 6 per genotype). Immunohistochemistry (IHC), *Dchs1*$^{+/-}$ (n = 5) anterior, posterior leaflets (AL, PL) exhibit myxomatous degeneration and expansion of proteoglycan expression compared to *Dchs1*$^{+/+}$ (n = 7), collagen (red), proteoglycans (green). MRI show posterior leaflet (PL) thickening in *Dchs1*$^{+/-}$ (arrow-inset) compared to control littermates. 3D reconstructions of MRI: *Dchs1*$^{+/-}$ mice exhibit thickened and elongated leaflets compared to *Dchs1*$^{+/+}$. (Two-tailed Student's *t*-test was used to calculate *P* values; *P* = 0.01, n = 4 per genotype).

thickening with quantitative increases in valve volume (Fig. 4 and Supplementary Video 8). All other echocardiographic measurements were unchanged (Extended Data Fig. 7). Histological and molecular characterization of *Dchs1*$^{+/-}$ mice confirmed leaflet thickening and showed myxomatous degeneration with increased proteoglycan accumulation in both mitral leaflets (Fig. 4). These results clearly show that *Dchs1* heterozygosity results in mitral valve prolapse in mice.

To determine if MVP has a developmental origin, we performed expression and functional analyses at embryonic and fetal time points. RNA *in situ* hybridization and immunohistochemistry showed expression of *Dchs1* in endocardial and mesenchymal cells of atrioventricular valve leaflets at all time points examined (Extended Data Fig. 8). While no morphological defects were observed in the *Dchs1*$^{+/-}$ mice during early embryonic development (E11.5–E13.5), at later time points (E15.5–E17.5) *Dchs1*$^{+/-}$ mice displayed changes in mitral-valve shape (Fig. 5a–c), which were more severe in *Dchs1*$^{-/-}$ animals. Histology and three-dimensional reconstructions of anterior and posterior mitral leaflets at E17.5 of *Dchs1*$^{+/+}$, *Dchs1*$^{+/-}$ and *Dchs1*$^{-/-}$ mice showed comparable leaflet volumes. However, *Dchs1*$^{+/-}$ and *Dchs1*$^{-/-}$ animals exhibited statistically significant changes in valve length and width (Supplementary Video 9 and Fig. 5a–c). In most leaflet regions measured, *Dchs1*$^{+/-}$ animals displayed an intermediate phenotype, demonstrating a gene dosage effect. These shape changes implicate *Dchs1* as critical for proper anatomical patterning of the valve, consistent with previous reports of *dachsous* function in the *Drosophila* wing[24]. Thus, *in vivo* lineage-tracing studies were performed on *Dchs1*$^{+/+}$ and *Dchs1*$^{+/-}$ mice. Crossing the *WT1-Cre/ROSA-eGFP*[25] line onto both *Dchs1*$^{+/+}$ and *Dchs1*$^{+/-}$ backgrounds allowed visualization of patterning defects of epicardial-derived cells (EPDCs) during migration into the posterior leaflet. This EPDC population initially migrates into the posterior leaflet as a sheet of cells. However, in the *Dchs1*$^{+/-}$ mice this sheet-like appearance is disrupted and an increase in EPDCs infiltrating diffusely throughout the valve tissue is observed (Extended Data Fig. 9a–c, Supplementary Video 10), concomitant with altered cellular patterning and alignment (Extended Data Fig. 9d, e). *In vitro* studies of MVICs from *Dchs1*$^{+/-}$ and from the family 2 MVP proband (p.R2330C) also show this increased migration phenotype (Extended Data Fig. 10a, b). Taken together, the mouse and human studies support a developmental aetiology for MVP, and invoke a model for MVP in which cell migration and patterning defects mediated by *DCHS1* contribute to disease pathogenesis.

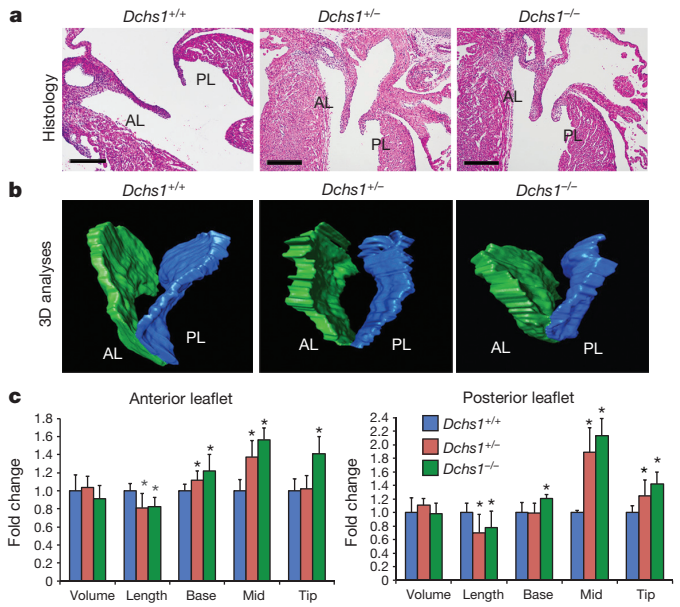

Figure 5 | Developmental aetiology for MVP. a, **b**, Haematoxylin and eosin and 3D reconstructions of E17.5 *Dchs1*$^{+/+}$, *Dchs1*$^{+/-}$ and *Dchs1*$^{-/-}$ mouse hearts showing thickening of anterior and posterior leaflets (AL, PL) in *Dchs1*$^{-/-}$ mice compared to *Dchs1*$^{+/+}$. *Dchs1*$^{+/-}$ valves display an intermediate phenotype. **c**, Quantification of valve dimensions showing *Dchs1*$^{-/-}$ (green bars) and *Dchs1*$^{+/-}$ (red bars) anterior and posterior lengths were significantly reduced compared to *Dchs1*$^{+/+}$ (blue bars) leaflets. *Dchs1*$^{-/-}$ and *Dchs1*$^{+/-}$ valves displayed increased thickness throughout the leaflets compared to *Dchs1*$^{+/+}$. Scale bars, 100 μm. $n = 5$ per genotype and two-tailed Student's *t*-test was used to calculate *P* values; $*P < 0.01$.

MVP is one of the most common cardiovascular diseases, affecting nearly 1 in 40 people worldwide[1–3]. Although its heritability and variable expression in large pedigrees has been known for decades, its genetic underpinnings have remained elusive[23,26]. We report the discovery of two loss-of-function mutations in *DCHS1* that segregate with MVP in three families. Our mouse models exhibit classical MVP, a phenotype that was traced back to developmental errors during valve morphogenesis. These findings provide a model for understanding inherited non-syndromic MVP as a developmentally based disease that progresses over the lifespan of affected individuals, consistent with previous reports on the natural history of MVP[27]. A robust estimate of the total contribution of rare *DCHS1* genetic variation to sporadic MVP has yet to be determined and will require sequencing of large cohorts of MVP patients. Nonetheless, discovery of this novel mechanistic pathway elucidated by intensively studying rare familial mutations will facilitate the identification of additional MVP genes and reveal pathogenic mechanisms that hold the potential for pre-surgical therapy for this very common cardiac disease.

Online Content Methods, along with any additional Extended Data display items and Source Data, are available in the online version of the paper; references unique to these sections appear only in the online paper.

Received 23 December 2014; accepted 17 June 2015.
Published online 10 August 2015.

1. Freed, L. A. *et al.* Mitral valve prolapse in the general population: the benign nature of echocardiographic features in the Framingham Heart Study. *J. Am. Coll. Cardiol.* **40,** 1298–1304 (2002).
2. Avierinos, J. F. *et al.* Natural history of asymptomatic mitral valve prolapse in the community. *Circulation* **106,** 1355–1361 (2002).
3. Freed, L. A. *et al.* Prevalence and clinical outcome of mitral-valve prolapse. *N. Engl. J. Med.* **341,** 1–7 (1999).
4. Vaishnava, P., Fuster, V., Goldman, M. & Bonow, R. O. Surgery for asymptomatic degenerative aortic and mitral valve disease. *Nat. Rev. Cardiol.* **8,** 173–177 (2011).
5. Waller, B. F., Maron, B. J., Del Negro, A. A., Gottdiener, J. S. & Roberts, W. C. Frequency and significance of M-mode echocardiographic evidence of mitral valve prolapse in clinically isolated pure mitral regurgitation: analysis of 65 patients having mitral valve replacement. *Am. J. Cardiol.* **53,** 139–147 (1984).
6. Freed, L. A. *et al.* A locus for autosomal dominant mitral valve prolapse on chromosome 11p15.4. *Am. J. Hum. Genet.* **72,** 1551–1559 (2003).
7. Levine, R. A. *et al.* Three-dimensional echocardiographic reconstruction of the mitral valve, with implications for the diagnosis of mitral valve prolapse. *Circulation* **80,** 589–598 (1989).
8. Levine, R. A., Stathogiannis, E., Newell, J. B., Harrigan, P. & Weyman, A. E. Reconsideration of echocardiographic standards for mitral valve prolapse: lack of association between leaflet displacement isolated to the apical four chamber view and independent echocardiographic evidence of abnormality. *J. Am. Coll. Cardiol.* **11,** 1010–1019 (1988).
9. Perloff, J. K. & Child, J. S. Clinical and epidemiologic issues in mitral valve prolapse: overview and perspective. *Am. Heart J.* **113,** 1324–1332 (1987).
10. Clark, H. F. *et al. Dachsous* encodes a member of the cadherin superfamily that controls imaginal disc morphogenesis in *Drosophila*. *Genes Dev.* **9,** 1530–1542 (1995).
11. Adzhubei, I. A. *et al.* A method and server for predicting damaging missense mutations. *Nature Methods* **7,** 248–249 (2010).
12. Chun, S. & Fay, J. C. Identification of deleterious mutations within three human genomes. *Genome Res.* **19,** 1553–1561 (2009).
13. Schwarz, J. M., Rodelsperger, C., Schuelke, M. & Seelow, D. MutationTaster evaluates disease-causing potential of sequence alterations. *Nature Methods* **7,** 575–576 (2010).
14. Visel, A., Thaller, C. & Eichele, G. GenePaint.org: an atlas of gene expression patterns in the mouse embryo. *Nucleic Acids Res.* **32,** D552–D556 (2004).
15. Guénette, S. *et al.* Essential roles for the FE65 amyloid precursor protein-interacting proteins in brain development. *EMBO J.* **25,** 420–431 (2006).
16. Margolin, D. H. *et al.* Ataxia, dementia, and hypogonadotropism caused by disordered ubiquitination. *N. Engl. J. Med.* **368,** 1992–2003 (2013).
17. Golzio, C. *et al. KCTD13* is a major driver of mirrored neuroanatomical phenotypes of the 16p11.2 copy number variant. *Nature* **485,** 363–367 (2012).

18. Chaki, M. *et al.* Exome capture reveals *ZNF423* and *CEP164* mutations, linking renal ciliopathies to DNA damage response signaling. *Cell* **150,** 533–548 (2012).
19. Norris, R. A. *et al.* Expression of the familial cardiac valvular dystrophy gene, filamin-A, during heart morphogenesis. *Dev. Dyn.* **239,** 2118–2127 (2010).
20. Rabkin, E. *et al.* Activated interstitial myofibroblasts express catabolic enzymes and mediate matrix remodeling in myxomatous heart valves. *Circulation* **104,** 2525–2532 (2001).
21. Nesta, F. *et al.* Leaflet concavity: a rapid visual clue to the presence and mechanism of functional mitral regurgitation. *J. Am. Soc. Echocardiogr.* **16,** 1301–1308 (2003).
22. Mao, Y. *et al.* Characterization of a *Dchs1* mutant mouse reveals requirements for Dchs1-Fat4 signaling during mammalian development. *Development* **138,** 947–957 (2011).
23. Nesta, F. *et al.* New locus for autosomal dominant mitral valve prolapse on chromosome 13: clinical insights from genetic studies. *Circulation* **112,** 2022–2030 (2005).
24. Cho, E. & Irvine, K. D. Action of *fat*, *four-jointed*, *dachsous* and *dachs* in distal-to-proximal wing signaling. *Development* **131,** 4489–4500 (2004).
25. Wessels, A. *et al.* Epicardially-derived fibroblasts and their contribution to the parietal leaflets of the atrioventricular valves in the murine heart. *Dev. Biol.* **366,** 111–124 (2012).
26. Zuppiroli, A., Roman, M. J., O'Grady, M. & Devereux, R. B. A family study of anterior mitral leaflet thickness and mitral valve prolapse. *Am. J. Cardiol.* **82,** 823–826 A10 (1998).
27. Kolibash, A. J. Jr *et al.* Evidence for progression from mild to severe mitral regurgitation in mitral valve prolapse. *Am. J. Cardiol.* **58,** 762–767 (1986).

Supplementary Information is available in the online version of the paper.

Acknowledgements This work was supported by the Fondation Leducq (Paris, France) Mitral Transatlantic Network of Excellence grant 07CVD04. MVP patient studies were supported by an Innovation in Clinical Research award of the Doris Duke Charitable Foundation, by an award of the Aetna Quality Care Research Fund, and by a gift from Rena M. Shulsky, New York, New York (S.A.S. and R.A.L.). Sequencing of the candidate region was performed at the Venter Institute through a grant from the National Heart Lung and Blood Institute Resequencing and Genotyping (RS&G) Service (S.A.S.). The work at MUSC was performed in a facility constructed with support from the National Institutes of Health, Grant Number C06 RR018823 from the Extramural Research Facilities Program of the National Center for Research Resources. Collection of the MVP France cohort was supported by the French Society of Cardiology. Other funding sources: National Heart Lung and Blood Institute: R01HL122906-01 (A.W.), R01-HL33756 (R.R.M.), COBRE 1P30 GM103342 (R.R.M., R.A.N., A.W.), 8P20 GM103444-07 (R.R.M. and R.A.N.), R01-HL109004 (D.J.M.), R01-HL127692 (D.J.M., S.A.S., R.A.N., R.A.L.); RO1-HL095696 (D.R.M.), VA Merit Review BX002327 (D.R.M.); National Institute of Mental Health R00-MH095867 (M.E.T.) The Hassenfeld Scholar Program (D.J.M.); The March of Dimes (M.E.T.); M.G.H. Scholars Program (S.A.S., M.E.T.); American Heart Association: 09GRNT2060075 (A.W.), 11SDG5270006 (R.A.N.), 2261354 (D.J.M.), 15GRNT25080052 (R.A.N.); National Science Foundation: EPS-0903795 (R.R.M.); NHLBI K24 HL67434, R01HL72265 and R01HL109506 and the Ellison Foundation, Boston, MA (R.A.L.), Howard Hughes Medical Institute (K.D.I.), and a gift from Michael Zak (D.J.M.). Thanks to T. Brown (MUSC) for his guidance on MRI studies, C. Hanscom (M.G.H.) for assistance with genomic libraries, and E. Lim (H.M.S.) for contributions in interpreting the exome mutation data. The authors would like to thank the Exome Aggregation Consortium and the groups that provided exome variant data for comparison. A full list of contributing groups can be found at http://exac.broadinstitute.org/about.

Author Contributions R.D., M.L., C.S., C.J., M.P., X.J., J.-J.S., D.T., S.O., X.E., F.C., and S.A.S. participated in genetic analysis, sequencing and mutation cloning. R.D., F.N.D., L.A.F., T.L.T., H.L.M., L.F.-F., J.S., C.T., R.A.L., and A.H. participated in patient collection and phenotyping using echocardiography. D.S.P., S.N.L. and D.J.M. performed zebrafish and cell culture experiments. M.E.T., M.R.S., N.B.N., C.D., H.B. and C.C. performed bioinformatics and statistical analysis. A.C., P.C., and P.B. established human patient cell cultures and histology on human tissues. A.d.V., K.W., K.D.I., Y.M., K.S., A.W., T.M., K.T., R.R.M. and R.A.N. performed mouse embryo and knockout experiments and cell alignment and migration assays. X.N., A.-M.B., D.R.M., H.K. performed mouse *in vivo* imaging. R.D., D.J.M., R.A.L., R.A.N. and S.A.S. wrote the manuscript. R.A.L., A.H., S.A.S. and J.J.S. coordinated the Leducq Mitral Network.

Author Information Reprints and permissions information is available at www.nature.com/reprints. The authors declare no competing financial interests. Readers are welcome to comment on the online version of the paper. Correspondence and requests for materials should be addressed to S.A.S. (slaugenhaupt@chgr.mgh.harvard.edu) or R.A.N. (norrisra@musc.edu).

METHODS

Study participants. Family 1 was originally recruited through the Echocardiography Laboratory at Massachusetts General Hospital as part of a phenotype-driven genetic study of MVP. MVP was diagnosed by specific criteria (>2 mm atrial leaflet displacement in a parasternal long-axis view)[6–9]. The study was approved by the Institutional Review Board of Partners Healthcare, Boston, Massachusetts, and all participants provided written informed consent. Complete details of the linkage analysis on this large, multigenerational family have been previously published[6]. In brief, the family contains 41 individuals in five generations. Echocardiograms and DNA were obtained on 28 subjects, of whom 12 were diagnosed with MVP, three were classified as having nondiagnostic minimal leaflet displacement, and 13 were unaffected[6]. Three patients had non-diagnostic valve leaflet displacement and were considered unknown for the original linkage analysis. The proband had prominent MVP with thickened leaflets, severe mitral regurgitation, and heart failure ultimately requiring surgical valve repair (Fig. 1c and Supplementary Videos 1–3). Other affected members also showed diffuse leaflet thickening, prolapse, and mitral regurgitation of varying severity; one required surgical repair. No extracardiac manifestations of connective-tissue abnormalities or Marfan syndrome were present in any family members. Following a complete genome scan, parametric and non-parametric analyses confirmed linkage of this family to a 4.3 cM region of chromosome 11p15.4. Consistent with the model of sex- and age-dependent penetrance, several of the unaffected members who carried the MVP allele were less than 15 years old at the time of evaluation (Fig. 1a). Importantly, an analysis using only affected individuals confirmed the linkage result.

DNA sequencing and variant calling in family 1. In order to identify the mutation, four affected individuals who shared the disease haplotype were chosen for sequencing (Fig. 1a). To reduce the likelihood of random haplotype sharing, we selected individuals with four distinct haplotypes on the non-MVP allele. A 2.1 Mb region of human chromosome 11 (5094774–7248926; NCBI36 coordinates) was targeted and screened for repetitive regions using the SureSelect system (Agilent). DNA extraction was performed using the AutoGenFlex STAR automated system (Autogen) and FlexiGen DNA purification reagents (Qiagen) according to the manufacturers' instructions. Bait oligonucleotides were designed to the non-repetitive regions of the targeted linkage peak, resulting in 1.03 Mb of target sequence using the SureSelect in-solution long RNA baits (Agilent). Captured DNA was amplified and quantified using the Agilent High Sensitivity DNA Kit for the Agilent 2100 Bioanalyzer, and sequenced using Illumina sequencing chemistry (paired-end, 100 cycles) at the Venter Institute supported by the NHLBI Resequencing and Genotyping Program. One hundred bases were sequenced from each end of the captured DNA fragments. Image analysis and base calling were performed using Illumina's GA Pipeline version 1.6.0. Sequence reads were mapped to the human genome (ncbi36) and variants identified using clc-ngs-cell-2.0.5-linux_64 (clc_ref_assemble_long -q -p fb ss 180 360 –I –r, and find_variations -c 8 -v -f 0.2). Variants were classified using VariantClassifier[28]. 4,891 SNVs were identified in the four subjects, 1,951 were shared by all four subjects. We classified all rare SNVs or those of unknown frequency based on conservation data, population genetic data, and predictive functional impact from public resources. We performed analyses of conservation of the variant locus using PhyloP[29], PhastCONS[30] and GERP[31], and assessed the population frequency initially using the Exome Variant Server, NHLBI GO Exome Sequencing Project (ESP), Seattle, Washington (http://evs.gs.washington.edu/EVS/) as an initial filter and the 1000 Genomes Project[32] as a secondary filter, cognizant of the limitations of the low-depth coverage of the 1000 Genomes Project to characterize rare mutations, which were available during our initial analyses.

Sporadic MVP patient cohort. As part of an international consortium on mitral valve disease, we initiated collection of MVP patients with the eventual goal of performing GWAS studies in MVP. To date, 1,896 patients have been collected in the United States, France, and Spain. MVP was defined as systolic displacement of one or both mitral leaflets ≥ 2mm beyond the annulus in parasternal or apical long-axis views, asymmetric posterior leaflet prolapse was also included in any view, including apical 4-chamber, when confirmed by side-to-side long-axis scanning[7,8]. Patients were required to have no evidence by history, physical examination, or imaging for Marfan syndrome or other connective tissue disorders associated with MVP.

Exome sequencing, genotyping, and variant evaluation. As part of an MVP exome sequencing pilot project conducted by the Leducq Mitral Network, exome data were generated on twenty-one severe, early onset MVP patients and made available to identify variants in *DCHS1*. Fifteen patients were collected in Paris and had severe bileaflet mitral valve prolapse with myxomatous leaflets and an average age of onset of 15 years. Six patients were collected in Nantes, France, and had similar clinical characteristics with an average age at onset of 42. Exome capture was carried out using the SureSelect Human All Exon System using the manufacturer's protocol version 1.0 that is compatible with Illumina paired-end sequencing. Exome-enriched genomes were multiplexed by flow cell for 101-bp paired-end read sequencing according to the protocol for the Hiseq 2000 sequencer (version 1.7.0; Illumina) to allow a minimum coverage of 30×. Reads were aligned to the human reference genome (UCSC NCBI36/hg19) using the Burrows-Wheeler Aligner (version 0.5.9). Evaluation of the *DCHS1* gene yielded 4 novel coding sequence variants that confirmed following repeat Sanger sequencing: 6646587 G/A (p.R2330C) 6646709 G/A (p.A2289V), 6648584 C/T (p.A1896T), 6648820 A/G (p.V1817A), base pair positions are NCBI36 coordinates. These four variants, in addition to the variants identified in family 1, were genotyped using Sequenom technology in the sporadic cohort. The major steps included primer and multiplex assay design using Sequenom's MassARRAY Designer software, DNA amplification by PCR, post-PCR nucleotide deactivation using shrimp alkaline phosphatase (SAP) to remove phosphate groups from unincorporated dNTPs, single-base extension reaction for allele differentiation, salt removal using ion-exchange resin, and mass correlated genotype calling using SpectroCHIP array and MALDI-TOF mass spectrometry. Quality control to determine sample and genotyping quality and to potentially remove poor SNPs and/or samples was performed in PLINK, a whole genome association analysis toolset. We predicted the impact on gene function using PolyPhen2[11], Mutation Taster[13] and LRT[12].

Identification of family 2 and 3. In order to identify other mutations in *DCHS1*, we first evaluated *DCHS1* in the exome sequence data described above, reasoning that early onset forms may be more likely to have strong genetic aetiologies. Rare variants causing amino acid substitutions in *DCHS1* were identified in four individuals (p.V1817A, p.A1896T, p.A2289V, and p.R2330C) and genotyped in a cohort of 1,864 sporadic MVP patients that included the 21 individuals with exome data; two of these variants, both localized to exon 19, were observed in the MVP cohort (p.A2289V in two cases and p.R2330C in three cases). The proband in family 2 carried the p.R2330C variant and underwent surgery for MVP in Paris. We were able to collect DNA and echocardiograms on first-degree relatives at that time. Additional clinical characteristics of the proband in family 2 included congestive heart failure (NYHA II/III) with left ventricular dilatation (70/50 mm end-diastolic/end-systolic dimensions), impaired left ventricular systolic function (ejection fraction 53%, low for this volume overload), recurrent symptomatic atrial fibrillation, non-sustained ventricular tachycardia, and exercise-induced pulmonary hypertension (70 mm Hg systolic). The proband in family 3 was originally collected in Amiens, France. All echocardiograms were read in both Boston and Paris and readers were blind to genotype data.

***D. rerio* studies.** Husbandry, knockdown and expression analyses were performed in the wild-type *D. rerio* (zebrafish) strain Tubingen AB. Morpholinos were injected at a dose of 1.5 ng (after dose optimization) into single-cell embryos to achieve gene knockdown, and phenotypes were examined at 48 and 72 h post-fertilization in three separate experiments of 50–75 embryos and compared to controls using Fisher's exact test. Morpholino GeneTools LLC (Philomath, OR) sequences were as follows: *apbb1* AACAAAGCGTACCACTCAGATTAGC, *dchs1a* TAAAGAAATGACAGTCCTACCTCCA, and *dchs1b* CATAACTGTT AAGAGTTCCGCTACA. Knockdown was confirmed by quantitative polymerase chain reaction. qPCR was performed as previously described[33]. In brief, 20–30 morpholino-injected embryos were collected at 72 hpf, and snap frozen in liquid nitrogen. TRIzol (Sigma) was added, RNA was purified according to the manufacturer's instructions, and cDNA was prepared using a Superscript III Kit (Invitrogen). Primer sets were as follows: *apbb1*, 5′-GTGGAGGCGAGAACA GAG, 5′-CCAGCAGGAAGATCCGTGTC; *dchs1a*, 5′-GTTTCATGGAGGTT ACAGC, 5′-CTTAATCCACCCCCATCCAC; *dchs1b*, 5′-GTTTCCTTGAGG TAAAGGCGG, 5′-GGCCACCCCCATCGGACG. qPCR was performed using SYBR Green (Applied Biosystems) in triplicate on an Applied Biosystems 7500 Fast Real-Time PCR instrument and normalized against β-actin. All zebrafish experiments were performed under protocols approved by the Institutional Animal Care and Use Committee at Massachusetts General Hospital.

***D. rerio in situ* hybridizations.** *In situ* hybridizations were performed as previously described[34] using a partial clone of *dchs1b* (Open Biosystems, Clone ID 7136458) amplified with primers containing a T7 RNA polymerase site engineered onto the 3′ end of the reverse primer (Forward 5′-GGCAGTTCAA GTGGTGGT. Reverse: TAATACGACTCACTATAGGGTTAAATCCTCATCT CAGCCTCA, T7 site underlined.) The *dchs1b* probe was produced using a T7 RNA polymerase (Ambion) and digoxigenin-labelled dNTPs (Roche). Other riboprobes used in the study have been previously described[35].

Generation of *DCHS1* expression constructs. Human *DCHS1* and the mutant containing the c.590C>T and c.7538G>A sequence changes were synthesized by Integrated DNA Technologies. A unique EcoRI site, a T7 polymerase site, and a Kozak sequence were added to the 5′ end of each gene, while a V5 tag and unique Xho1 site were added to the 3′ end. Each gene was then subcloned into the expression vector pcDNA3.1. Additional expression constructs were generated

that contained only the c.590C>T (p.P197L) mutation or only the c.7538G>A (p.R2513H) mutation. These constructs were made using the QuikChange II XL Site-Directed Mutagenesis Kit (Agilent Technologies) as per the manufacturer's instructions. The P197L construct was generated from the double mutant construct by changing the R2513H (c.7538G>A) mutation back into the wild type sequence using the following primers: 5′-gctgatggaagcc**g**cagccatgccgct, 3′-agcggc atggctg**c**ggcttccatcagc. (The underlined bold base indicates the base pair changed.) The R2513H construct was generated by introducing the (c.7538G>A) mutation into the wild type *DCHS1* construct using the following primers: 5′-gctgatggaagcc **a**cagccatgccgct, 3′-agcggcatggctg**t**ggcttccatcagc.

Preparation and injection of *DCHS1* mRNA. mRNA was prepared from the wild-type *DCHS1* and *DCHS1* mutant expression vectors using a T7 mMessage mMachine Kit (Ambion) according to the manufacturer's instructions. Injection mixtures containing 0.75 ng *dchs1b* MO alone, or 0.75 ng *dchs1b* MO plus 7 fg μl^{-1} of human *DCHS1* mRNA (either wild type or mutant) were injected into one-cell embryos, and fish were scored for atrioventricular canal defects (failure to loop, and presence of regurgitation) 72 h later. Data were collected from three independent experiments performed with 20–30 embryos each and comparisons made using Fisher's Exact test.

Isolation of DCHS1 p.R2330C MVP and control patient mitral valve tissue and valvular interstitial cells. Resected posterior mitral valve tissue was used for culture and histology. For culture, valve pieces were minced in phosphate buffered saline (PBS) and washed in DMEM with antibiotics (penicillin/streptomycin (P/S) and fungizone) and incubated in DMEM with collagenase type II (Worthington) (1 mg ml^{-1}) at 37 °C for 12 h. Following mechanical dissociation in DMEM, the cell suspension was filtered through a 40-μm cell strainer and cells were cultured in DMEM with 15% fetal calf serum and antibiotics (P/S, fungizone). Although rare valve endothelial cells were present at P0, only cells with a fibroblastic phenotype (VICs) remained following P1-2. For all experiments, these valvular interstitial cells were used before passage 5. For histology: valves were fixed in formalin, embedded in paraffin and sectioned at 5 μm. Movat's Pentachrome histological stain was performed using standard procedures.

Cell culture studies. Wild type, p.P197L, p.R2513H and p.P197L/R2513H *DCHS1* constructs were either synthesized by Integrated DNA Technologies or generated by site-directed mutagenesis (as described above), with an amino-terminal V5 epitope tag. Except where indicated, "mutant *DCHS1*" indicates the double mutant p.P197L/p.R2513H haplotype in family 1. These constructs were expressed in mycoplasma-free HEK293 cells (ATCC, not independently authenticated) using cationic lipid-mediated transient transfection (Lipofectamine LTX, Invitrogen). Protein expression of transfected HEK cells was measured by quantifying western blots using an antibody to the V5 epitope tag (Invitrogen). Patient cells: for patient cells, control and p.R2330C valvular interstitial fibroblasts from posterior leaflets were plated at 2.5×10^4 cells in a 24-well dish. 24 h later, protein stability experiments were performed. Protein stability experiments involved addition of cycloheximide 24 h after transfection (WT and p.R2513H transfectants) or plating (control or p.R2330C patient cells). For the cycloheximide experiments, media containing 100 ng ml^{-1} of cycloheximide was added at 24 h post-transfection and each well was harvested as above at the indicated time points. Western blots were probed with either a mouse anti-V5 primary antibody (1:4,000 dilution Invitrogen) or a rabbit anti-*Dchs1* antibody[36](1:1,500 dilution), and an HRP-linked secondary at the same dilution (Thermo Scientific). Blots were also probed with a mouse anti-tubulin primary (Millipore) at a 1:4,000 dilution, and the same secondary antibody as above. Blots were treated with Pierce ECL Substrate and visualized on film. For quantitation, blot pixel intensity was measured by ImageJ (NIH), and normalized to tubulin. Each sample was run in triplicate, and a regression curve was fit and half-lives calculated using SigmaPlot 12.

Mouse studies. Dchs1 mice and genotyping were previously described[22]. All mice were blinded for genotype. Following phenotypic analyses, the genotypes of each sample were matched with the experimentally determined data sets. Histology, mitral valve analyses (echocardiography, MRI, and morphometric determination), and expression studies were performed on embryonic and adult (9-month male) wild-type (*Dchs1*$^{+/+}$), heterozygote (*Dchs1*$^{+/}$), and knockout (*Dchs1*$^{-/-}$) hearts (C57/Bl6;Sv129 mixed background). For histology: fetal (E17.5) and adult (9-month) hearts were processed for haematoxylin and eosin stainings and immunohistochemistry (IHC) as previously described[37]. For fetal analyses, *Dchs1*$^{+/+}$, *Dchs1*$^{+/-}$, and *Dchs1*$^{-/-}$ mice were analysed ($n = 5$ per genotype). Due to neonatal lethality of the *Dchs1*$^{-/-}$ mice and loss-of-function *Dchs1* mutations in humans, adult analyses were restricted to *Dchs1*$^{+/+}$ ($n = 7$) and *Dchs1*$^{+/-}$ ($n = 5$). For all analyses male mice were used. Antibodies used for IHC were: hyaluronan binding protein (HABP) to stain proteoglycans (1:100) (Calbiochem), collagen I (1:100) (MDbio), and Hoescht to stain nuclei (1:10,000) (Invitrogen). AMIRA 3D reconstructions were performed to generate volumetric measurements of fetal (E17.5) anterior and posterior mitral leaflets ($n = 5$ for each genotype) as previously described[38]. Length and width measurements of the mitral leaflets were obtained from histological sections. 25 consecutive 5 μm sections from anterior and posterior mitral leaflets of each genotype were used for measurements (*Dchs1*$^{+/+}$, $n = 4$, *Dchs1*$^{+/-}$, $n = 7$, *Dchs1*$^{-/-}$, $n = 5$). ImageJ software was used to measure the length of anterior and posterior leaflets from annulus to tip and the perpendicular width at the base, mid-region and tip. Measurements were compared to wild-type data to generate fold change and statistical significance ($P < 0.01$) was calculated using a Student's *t*-test. For quantification of mitral valve interstitial cell alignment: hearts were initially dissected from E17.5 fetuses. The apex of the heart was dissected and discarded followed by removal of the left atrium. A cut was made cranial to caudal along the anterior aspect of the myocardium. The left ventricle was reflected to gain visualization of the leaflets. The left ventricle and interventricular septum were pinned such to stretch the papillary muscle and the chords. This resulted in obtainment of the leaflet as a planar sheet of tissue. The tissue was fixed in this position to ensure the leaflet was maintained in this orientation, as failure to do so results in curling of the leaflet making measurements and plane of orientation inconsistent between animals. Once the planar leaflet tissue was fixed in 4% PFA for 5 min, the leaflet was released from the heart by cutting the chords and dissecting along the annulus fibrosae. The tissue was then processed through normal protocols and placed en-face on paraffin. This technique was performed blinded to genotype and performed in exactly the same manner for all valve isolates. Performing this type of dissection and tissue processing ensures that all leaflets are placed in nearly identically oriented planes. The vector maps and quantification of cell alignment were performed blinded by two independent researchers. Only after the data was generated did a third researcher perform the PCR genotyping. Vector maps were manually generated as previously described[39]. Cells that deviated >10 degrees from an average alignment plane were counted as misaligned. Interstitial cells within anterior leaflets from each genotype were measured. Total number of cells measured were: WT = 1,083, ($n = 4$); Het = 1,118, ($n = 4$); KO = 1,953, ($n = 4$). Statistical significance was calculated using a *Students t*-test with a P value < 0.05 being significant. Very little variation existed between the independent valves of each genotype as is graphically depicted. For mouse echocardiography the Vevo2100 imaging system (VisualSonics, Toronto, Canada) was used with 22–55 MHz linear transducer probe (MS550D) and used for 2-D B-mode and M-mode analysis. Heart rate was maintained at 400–500 bpm via isoflurane anaesthesia. The mitral valve leaflet was visualized and its function was assessed in parasternal long-axis B-mode view by placing the transducer on the left lateral chest wall. End-systolic and end-diastolic left ventricular dimensions and wall thicknesses were measured according to the American Society of Echocardiography guidelines as applied to mice. Left ventricular wall thickness was measured at the level of interventricular septum and the posterior wall. Left ventricular volume was calculated from Simpson's method of disks and ejection fraction determined from the formula (left ventricular end-diastolic-end-systolic volume)/(left ventricular end-diastolic volume). Offline image analyses were performed using dedicated VisualSonics Vevo2100 1.2.0 software. Mitral valve prolapse was determined based on superior systolic displacement of one or more leaflets above the line connecting the annular hinge points in the long-axis view ($n = 6$ per genotype). For MRI experiments: 9-month-old male *Dchs1*$^{+/+}$ and *Dchs1*$^{+/-}$ mice ($n = 4$) were sacrificed and the hearts were perfusion fixed and immersed 1:40 (12.5 mmol) Gadolinium (ProHance) in 10% formalin overnight before imaging. MRI was undertaken at 7T using a Bruker Biospin console (Pavavision 5.1) with a volume transmitter coil and a phased array surface coil. Gradient echo FLASH 3D images were collected with repetition time/echo time = 50 ms/5.4 ms, flip angle = 30°, number of excitations = 3, matrix = $256 \times 256 \times 256$ and pixel resolution = $55 \times 55 \times 59$ μm. Images in DICOM format were imported into AMIRA 3D reconstruction software and volume quantification were performed as described previously[38]. Pairwise comparison of littermates were performed and statistical significance was determined (Student's *t*-test) with $P < 0.01$. All mouse experiments were performed under protocols approved by the Institutional Animal Care and Use Committee, Medical University of South Carolina. Prior to cardiac resection, mice were euthanized in accordance with the Guide for the Care and Use of Laboratory Animals (NIH Publication No. 85-23, revised 1996).

RNA expression analyses of *Dchs1* and *Apbb1*. Section *in situ* hybridization was performed as previously described[40] on 4 embryos at each time point to localize *Dchs1* expressing cells throughout cardiac development. A *Dchs1* digoxigenin-labelled riboprobe (Roche) was generated against region 9222–10180 of accession number NM_00162943 and used for *in situ* hybridization at E11.5, E13.5, and E15.5. RNA *in situ* hybridization for *Apbb1* at E14.5 was performed through GenePaint[14]. Two separate riboprobes were used to analyse *Apbb1* RNA expression at E14.5. These probes were generated against regions 1676–2506 and 370–1967 of accession number NM_001253885.1. These probes span all known isoforms for *Apbb1* and provide similar spatial RNA expression patterns.

Protein expression. *Dchs1* antibodies were generated by immunizing rabbits with a synthetic peptide corresponding to rat Dchs1 protein sequence: CSTYMVES PDLVEADSAA (region 1308–1324 of accession number NP_001101014)[36]. Immunohistochemistry was performed as described previously[19] using a 1:100 dilution of primary antibody.

***In vivo* lineage trace.** To trace the fate of epicardially derived cells in *Dchs1*$^{+/+}$ and *Dchs1*$^{+/-}$ mitral leaflets, the Wt1/IRES/GFP-Cre mouse[25] was bred with the *Dchs1*$^{+/-}$ and *Dchs1*$^{+/+}$ mice ($n = 4$ per genotype). Mice were euthanized at neonatal day 0 (P0), hearts were isolated and fixed overnight at 4 °C in 4% paraformaldehyde dissolved in PBS. Hearts were processed through a series of graded ethanol, cleared in toluene, and embedded in Paraplast Plus (Fisherbrand, 23-021-400). Hearts were sectioned at 5 µm and slides were treated with 15 ml of antigen unmasking solution (Vector Biolabs, H-3300) in 1,600 ml of distilled water for 10 min in a pressure cooker (Cuisinart) followed by incubation for 1 h at room temperature with 1% BSA (Sigma, B4287) in PBS. Expression of EGFP after Cre recombination was detected by immunofluorescence using antibodies against GFP (Abcam, 13970) and myosin heavy chain (MF20; DSHB). 5 µm sections throughout the entire valve were used for 3D reconstructions using Amira software. The volume of GFP positive cells and the volume of each mitral leaflet were measured using this software. Cell counting was done on GFP positive and GFP negative cells every 15 µm throughout the entire valve. Pairwise comparison of littermates were performed and statistical significance was determined (Student's *t*-test) with $P = 0.04$ for posterior leaflet and $P = 0.86$ for anterior leaflet.

***In vitro* migration.** Human mitral valve interstitial cells were isolated from a control and the patient with the *DCHS1* mutation (p.R2230C) (proband family 2) and seeded into the Radius 24-well Cell Migration Assay plate containing hydrogels (Cell Biolabs, CBA-125). Cells were allowed to adhere overnight and then gels were dissolved. Wells were imaged over a period of 24 h and area of the cell free region was measured in Photoshop v.10.0.01 and subtracted from the initial area of the hydrogel to generate area migrated over time. Migration in the *Dchs1*$^{+/-}$ and *Dchs1*$^{+/+}$ mice was assessed by explanting P0 neonatal posterior mitral leaflets onto plastic. Images of the explants and migrating cells were captured at multiple time points. Distance migrated was measured as the distance from the explant to the farthest migrating cell. Measurements were taken at 5 points around the explant and averaged to calculate distance migrated. After 24 h, cells were fixed in ice-cold 100% methanol for 10 min and immunofluorescence was performed using an antibody against N-cadherin (1:1,000 dilution, BD Transduction Labs, 610920). Pairwise comparisons were performed and statistical significance was determined (Student's *t*-test) with $P < 0.05$.

Statistical considerations. In all experiments sample sizes were chosen to provide power of 0.8 to detect biologically significant differences between test groups with two-sided $\alpha = 0.05$. Specific statistical tests are listed in the methods for each individual experiment. Assumptions of normal distributions were made for quantitative biological measurements and comparison groups were assumed to have similar variances. For zebrafish experiments, fertilized oocytes were randomly selected within each clutch for injection with active compound versus controls. Mouse experiments were interpreted blinded to genotype.

28. Li, K. & Stockwell, T. B. VariantClassifier: a hierarchical variant classifier for annotated genomes. *BMC Res. Notes* **3,** 191 (2010).
29. Pollard, K. S., Hubisz, M. J., Rosenbloom, K. R. & Siepel, A. Detection of nonneutral substitution rates on mammalian phylogenies. *Genome Res.* **20,** 110–121 (2010).
30. Siepel, A. *et al.* Evolutionarily conserved elements in vertebrate, insect, worm, and yeast genomes. *Genome Res.* **15,** 1034–1050 (2005).
31. Cooper, G. M. *et al.* Distribution and intensity of constraint in mammalian genomic sequence. *Genome Res.* **15,** 901–913 (2005).
32. The 1000 Genomes Project Consortium. An integrated map of genetic variation from 1,092 human genomes. *Nature* **491,** 56–65 (2012).
33. Morrison, T. B., Weis, J. J. & Wittwer, C. T. Quantification of low-copy transcripts by continuous SYBR Green I monitoring during amplification. *Biotechniques* **24,** 954–958,–960, 962 (1998).
34. Thisse, B. *et al.* Spatial and temporal expression of the zebrafish genome by large-scale *in situ* hybridization screening. *Methods Cell Biol.* **77,** 505–519 (2004).
35. Kolpa, H. J. *et al.* miR-21 represses Pdcd4 during cardiac valvulogenesis. *Development* **140,** 2172–2180 (2013).
36. Tsukasaki, Y. *et al.* Giant cadherins Fat and Dachsous self-bend to organize properly spaced intercellular junctions. *Proc. Natl Acad. Sci. USA* **111,** 16011–16016 (2014).
37. Norris, R. A. *et al.* Periostin regulates atrioventricular valve maturation. *Dev. Biol.* **316,** 200–213 (2008).
38. Sauls, K. *et al.* Developmental basis for filamin-A-associated myxomatous mitral valve disease. *Cardiovasc. Res.* **96,** 109–119 (2012).
39. Xu, F., Beyazoglu, T., Hefner, E., Gurkan, U. A. & Demirci, U. Automated and adaptable quantification of cellular alignment from microscopic images for tissue engineering applications. *Tissue Eng. Part C Methods* **17,** 641–649 (2011).
40. Norris, R. A. *et al.* Identification and detection of the periostin gene in cardiac development. *Anat. Rec. A Discov. Mol. Cell. Evol. Biol.* **281A,** 1227–1233 (2004).

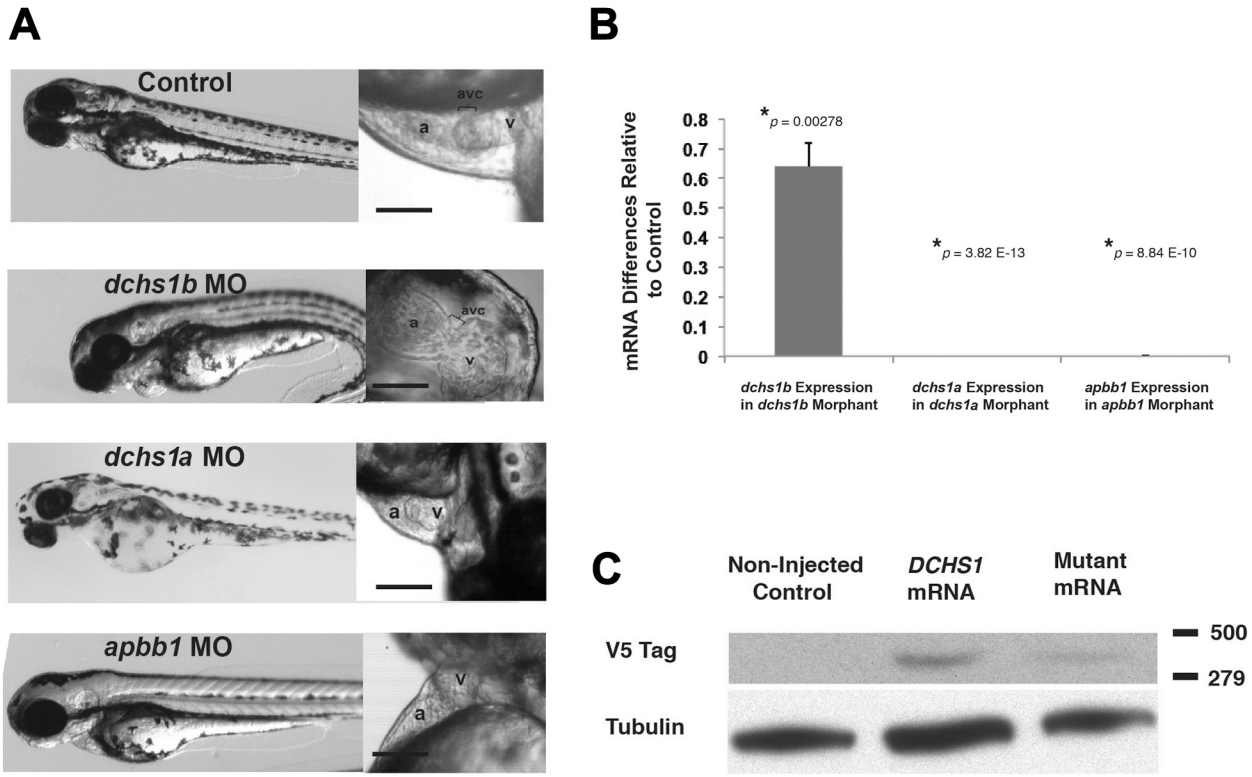

Extended Data Figure 1 | Measurement of endogenous and exogenous gene expression in *D. rerio*. **a**, Corresponding representative embryos of each morpholino knockdown on the left, with close-up of heart on the right. **b**, To assess efficiency of morpholino knockdown, 20 embryos were collected 72 h after injection, mRNA was collected, and quantitative PCR was performed with three technical replicates. We demonstrate that morpholino (MO) knockdown of each indicated gene results in reduced mRNA expression, after normalization to beta-actin expression, compared to mock-injected controls (two-sided Student's *t*-test). *P* values are noted on graphs. **c**, Western blotting of 20 pooled embryos injected with *DCHS1* mRNA demonstrates the production of protein. Mutant mRNA refers to the compound mutant P197L/R2513H.

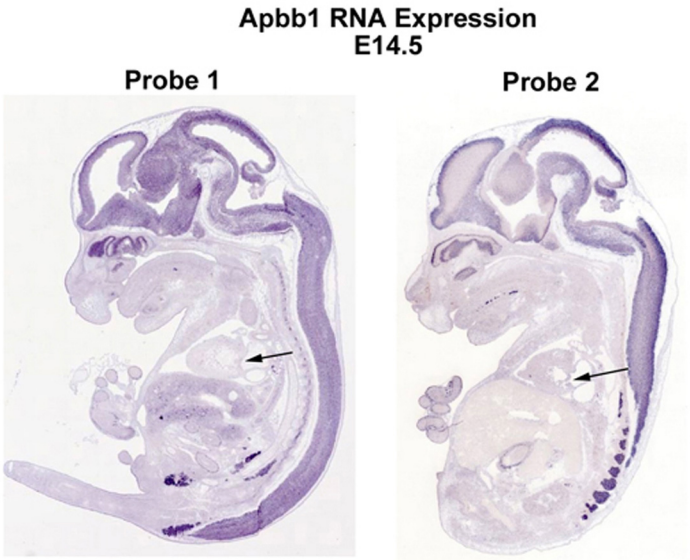

Extended Data Figure 2 | *Apbb1* is not expressed during cardiac morphogenesis. *Apbb1* RNA expression was analysed at E14.5 in sagittal sections using 2 separate antisense probes. Whereas strong cranial and neural expression is observed for *Apbb1*, no detectable cardiac expression or valve expression (arrow) is evident.

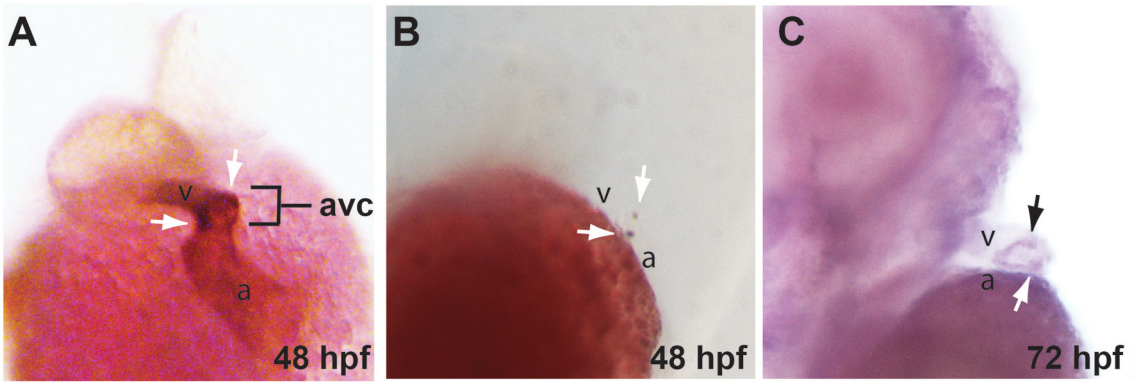

Extended Data Figure 3 | *Dachsous1b* expression at the atrioventricular junction. *In situ* hybridization reveals the presence of *dchs1b* in the atrioventricular canal (avc) at 54 hpf (**a**, **b**) and 72 hpf (**c**). The *dchs1b* expression is purple while a counterstain for cardiac tissue is brown (**a**). White arrows highlight the *dchs1b* signal in the atrioventricular canal.

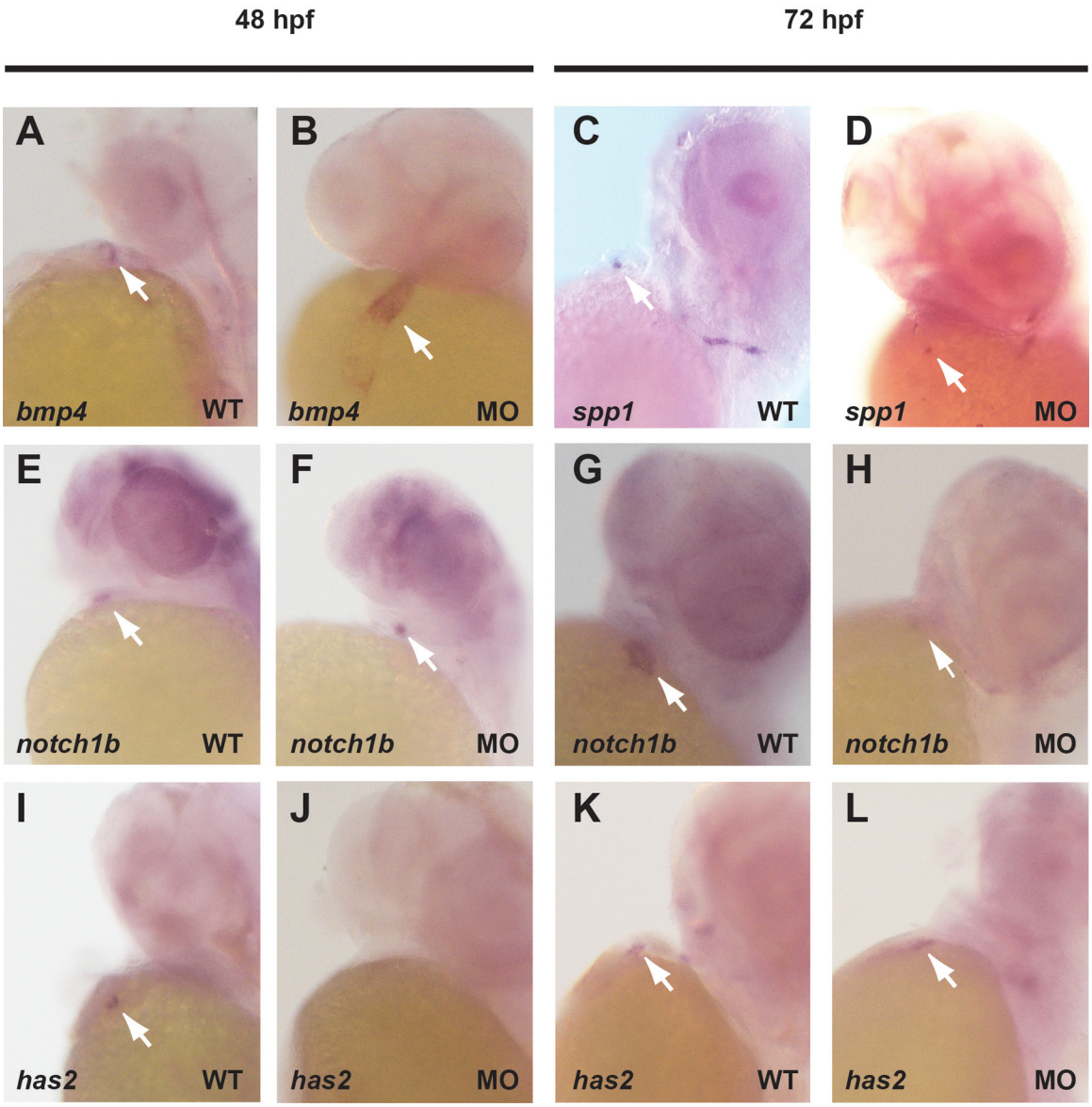

Extended Data Figure 4 | *Dachsous1b* knockdown alters atrioventricular ring markers. *In situ* hybridization at 48 hpf and 72 hpf, as indicated, was performed for known atrioventricular ring markers. In contrast to WT (**a**) *bmp4* expression is expanded into the ventricle at 48 hpf in *dchs1* knockdown embryos at 48 hpf (**b**), *spp1* and *notch1b* expression was largely unperturbed (**c**–**f**), and *has2* expression was not detected at 48 hpf, and is faint at 72 hpf in *dchs1* knockdown, compared to identically handled and stained controls (**i**–**l**).

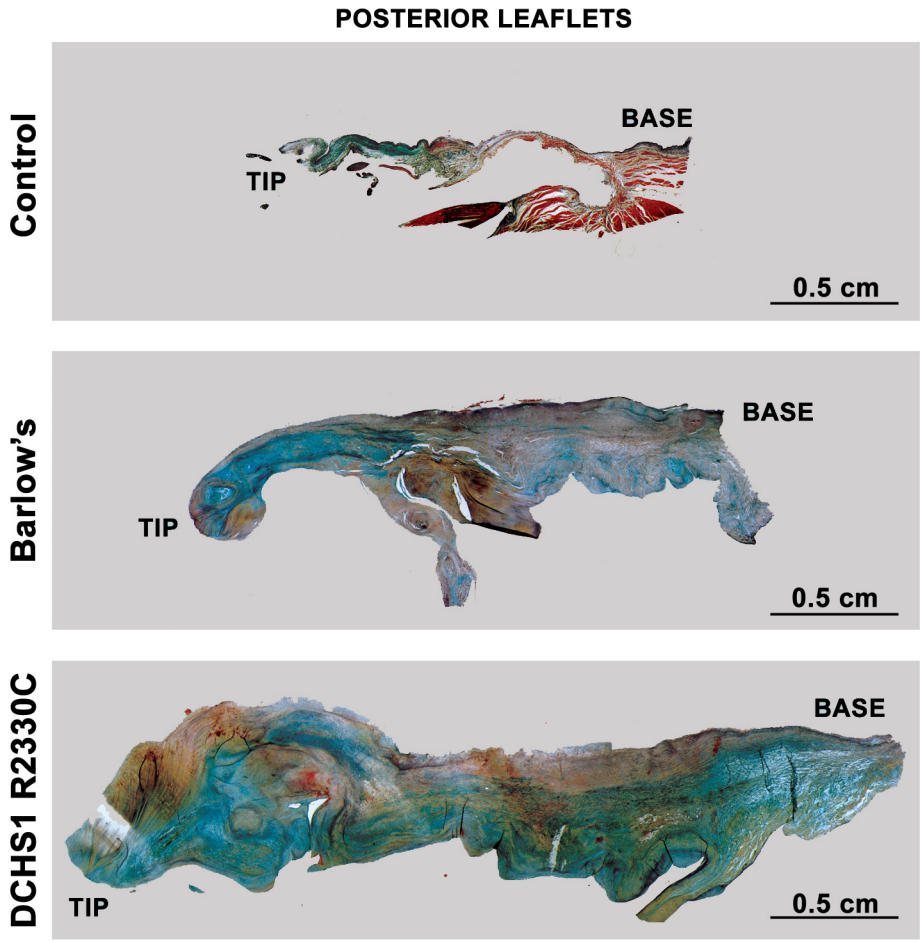

Extended Data Figure 5 | Histopathology mitral valves. Human posterior leaflets of control, Barlow's with MVP, and DCHS1 p.R2330C were isolated, fixed and stained with Movat's pentachrome. Leaflet thickening, elongation and myxomatous degeneration is observed in the Barlow's and DCHS1 p.R2330C leaflets compared to controls. Expansion of the proteoglycan layer (blue) and disruption of the normal stratification of matrix boundaries is observed in the Barlow's and DCHS1 p.R2330C leaflets. Blue, proteoglycan; yellow, collagen; black, elastin; red, fibrin or cardiac muscle. Scale bars, 0.5 cm.

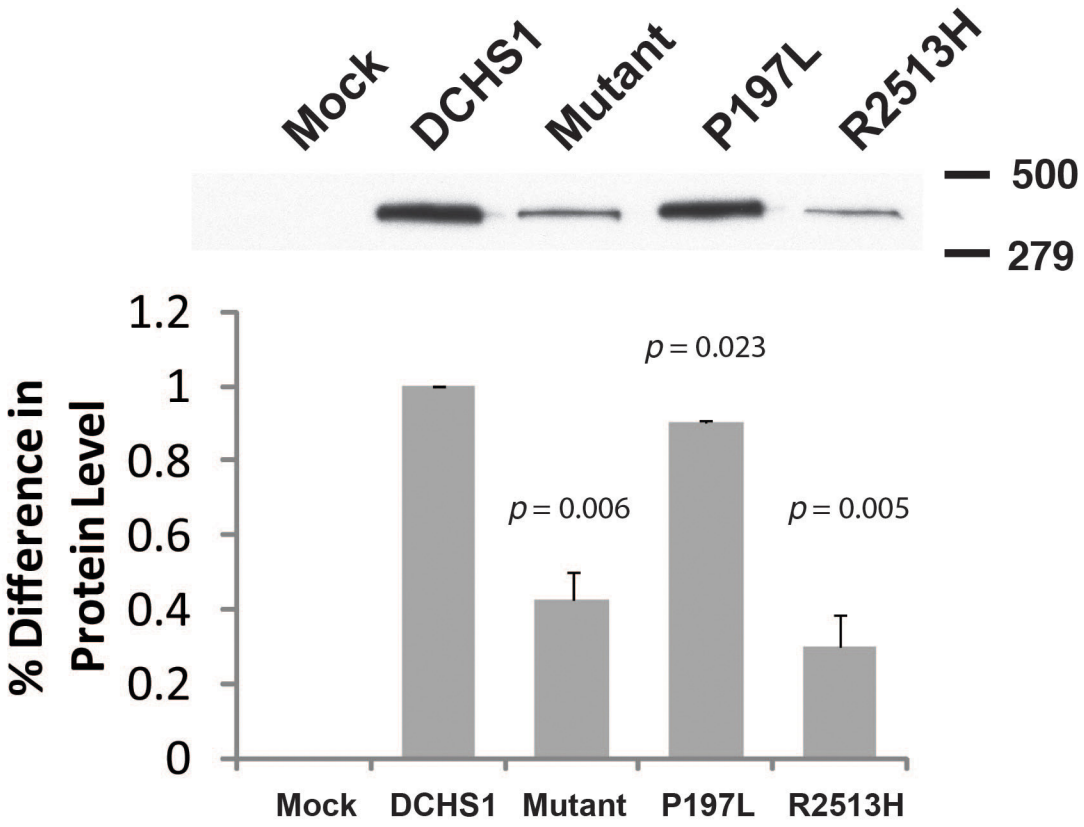

Extended Data Figure 6 | Protein expression of uncoupled mutations. In order to determine which family 1 *DCHS1* mutation is leading to the observed decrease in protein expression, constructs were generated that harboured only the p.P197L or the p.R2513H variant. Mutant refers to the double mutant P197L/R2513H construct. Western blot analyses from transfected HEK293 cells, three independent biological replicates, demonstrate that the p.R2513H mutation causes a significant decrease in *DCHS1* protein expression, similar to that of the construct with both variants (mutant), suggesting pathogenicity. Percent difference in protein levels is depicted. Normalization of data was accomplished by qPCR specific to the transfected constructs. *P* values from the Student's *t*-test are indicated in graphs.

Cardiac Function (Echocardiography)

	Measurement	Mode	Parameter	Units	Dchs1 +/+ (N=6)	STD	Dchs1 +/- (N=6)	STD	p-value
	IVS;d	M-Mode	Depth	mm	0.8208935	0.187955	0.9096155	0.140668	0.170463
	IVS;s	M-Mode	Depth	mm	1.290918667	0.243251	1.369591167	0.200513	0.393879
	LVID;d	M-Mode	Depth	mm	4.282772333	0.515571	4.045031833	0.217379	0.28511
	LVID;s	M-Mode	Depth	mm	2.887339833	0.33268	2.735737167	0.362674	0.544435
	LVPW;d	M-Mode	Depth	mm	0.914783667	0.210393	0.961298	0.215238	0.691322
	LVPW;s	M-Mode	Depth	mm	1.293790333	0.237193	1.385096	0.238861	0.252632
	Calculation		**Units**						
	EF		%		60.5315595	7.808571	61.0498945	8.235624	0.934765
	FS		%		32.317489	5.734886	32.5702855	5.939884	0.955876
	LV Mass		mg		148.9330448	42.74011	150.7559685	40.75343	0.891865
	LV Mass (Corrected)		mg		119.1464358	34.19209	120.6047747	32.60275	0.891865
	LV Vol;d		ul		83.76315083	23.58335	72.14675683	9.354702	0.261482
	LV Vol;s		ul		32.456727	9.786065	28.5946545	8.983466	0.570045

Extended Data Figure 7 | Cardiac function is not altered in *Dchs1*$^{+/-}$ mice. M-mode analyses were performed to determine whether cardiac structure and/or function were perturbed in the *Dchs1*$^{+/-}$ mice. No statistically significant differences were observed in either cardiac structure or calculated cardiac function ($n = 6$ for each genotype). IVS, interventricular septum; d, diastole; s, systole; LVID, left ventricular internal dimension; LVPW, left ventricular posterior wall; EF, ejection fraction; FS, fractional shortening; LV, left ventricle.

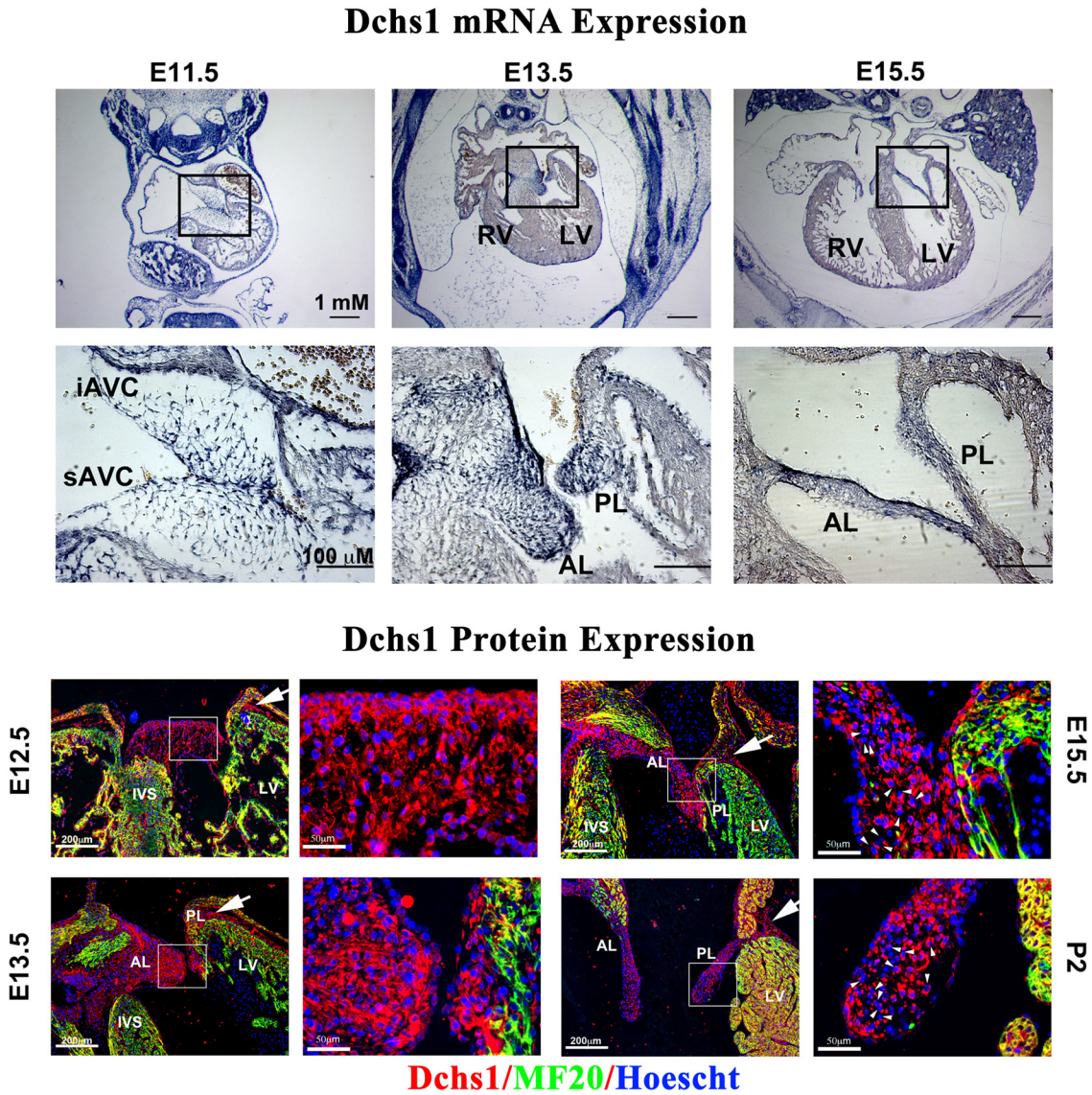

Extended Data Figure 8 | *Dchs1* expression during cardiac development. Top, RNA expression of *Dchs1* was analysed during embryonic gestation (E11.5, E13.5, and E15.5) by section *in situ* hybridization. At E11.5 *Dchs1* RNA (blue staining) expression is observed in the endocardium and mesenchyme of the superior and inferior cushions (sAVC and iAVC, respectively). A gradient pattern of expression is observed at this time point with more intense expression near the endocardium. At E13.5 and E15.5, a similar pattern is observed in the forming anterior and posterior mitral leaflets (AL and PL, respectively). Bottom, *Dchs1* protein expression (red) is observed throughout cardiac development in the endothelial cells and interstitial cells of the developing valves. *Dchs1* shows asymmetric expression in the valvular interstitial cell bodies around E15.5 (arrowheads). *Dchs1* protein is also observed in the epicardium and atrioventricular sulcus (arrows). (Red Dchs1; green MF20; blue Hoescht).

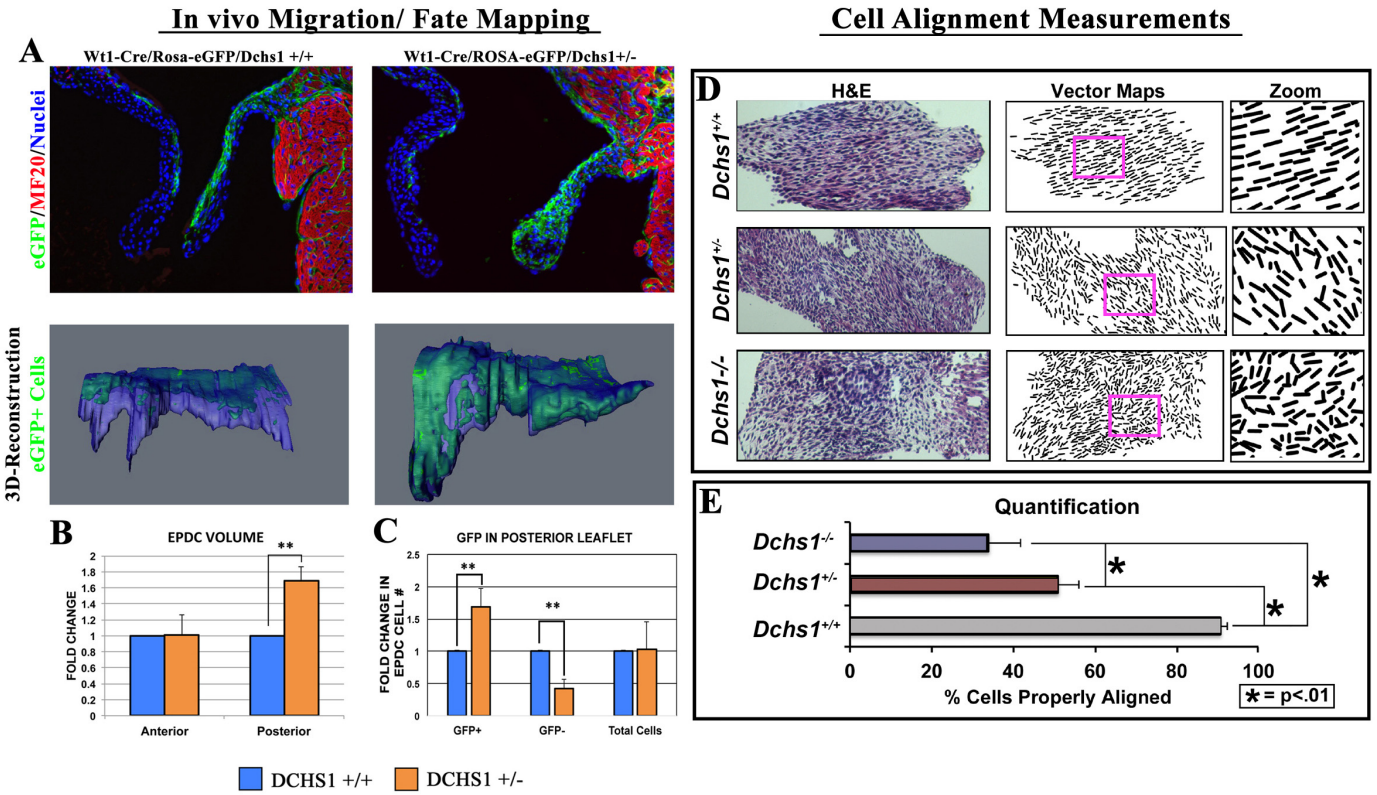

Extended Data Figure 9 | Dchs1 deficiency causes altered valvular interstitial cell patterning *in vivo*. **a**, IHC for eGFP of postnatal day 0 (P0) lineage traced *Wt1-Cre/Rosa-eGFP/Dchs1*$^{+/+}$ neonatal mice show epicardial-derived cells (EPDCs) migrating into the posterior leaflet as a sheet of cells directly under the endothelium of the atrialis. This normal patterning is perturbed in the *Wt1-Cre/Rose-eGFP/Dchs1*$^{+/-}$ mice. 3D reconstructions were used to examine all EPDCs in the posterior leaflet of both genotypes to obtain a complete fate map of these cells. **b**, **c**, Total volume of the leaflet is unchanged at this time point. However, the total volume of EPDCs as well as total EPDC cell number is significantly increased. There is a significant decrease in the number of non-EPDCs in the posterior leaflet with no overall change in total cell number. These data demonstrate that a minimum threshold of Dchs1 expression is required for normal migration of EPDCs into the posterior leaflet, normal patterning of this cell population, and cross-talk between EPDC and non-EPDC cell types in the valve. $^{**}P < 0.01$. **d**, Isolated anterior mitral leaflet from fetal (E17.5) *Dchs1*$^{+/+}$, *Dchs1*$^{+/-}$, and *Dchs1*$^{-/-}$ mice were used to quantify cellular alignment of valvular interstitial cells. Vector maps were generated from histological (haematoxylin and eosin) stains to show orientation and alignment of cells in relationship to each other. Boxes in each vector map panel are represented as zoomed images of regions within each of the valves to show cell orientation. **e**, Cell alignment and polarity were quantified as the number of cells that deviate >10 degrees from the proximal-distal (P–D) axis of the leaflet. 90% of the cells in *Dchs1*$^{+/+}$ show proper alignment with each other and along this P–D axis. Haploinsufficiency (*Dchs1*$^{+/-}$) results in a 50% reduction in cell alignment, which is further reduced in *Dchs1*$^{-/-}$ ($^{*}P$ values < 0.01).

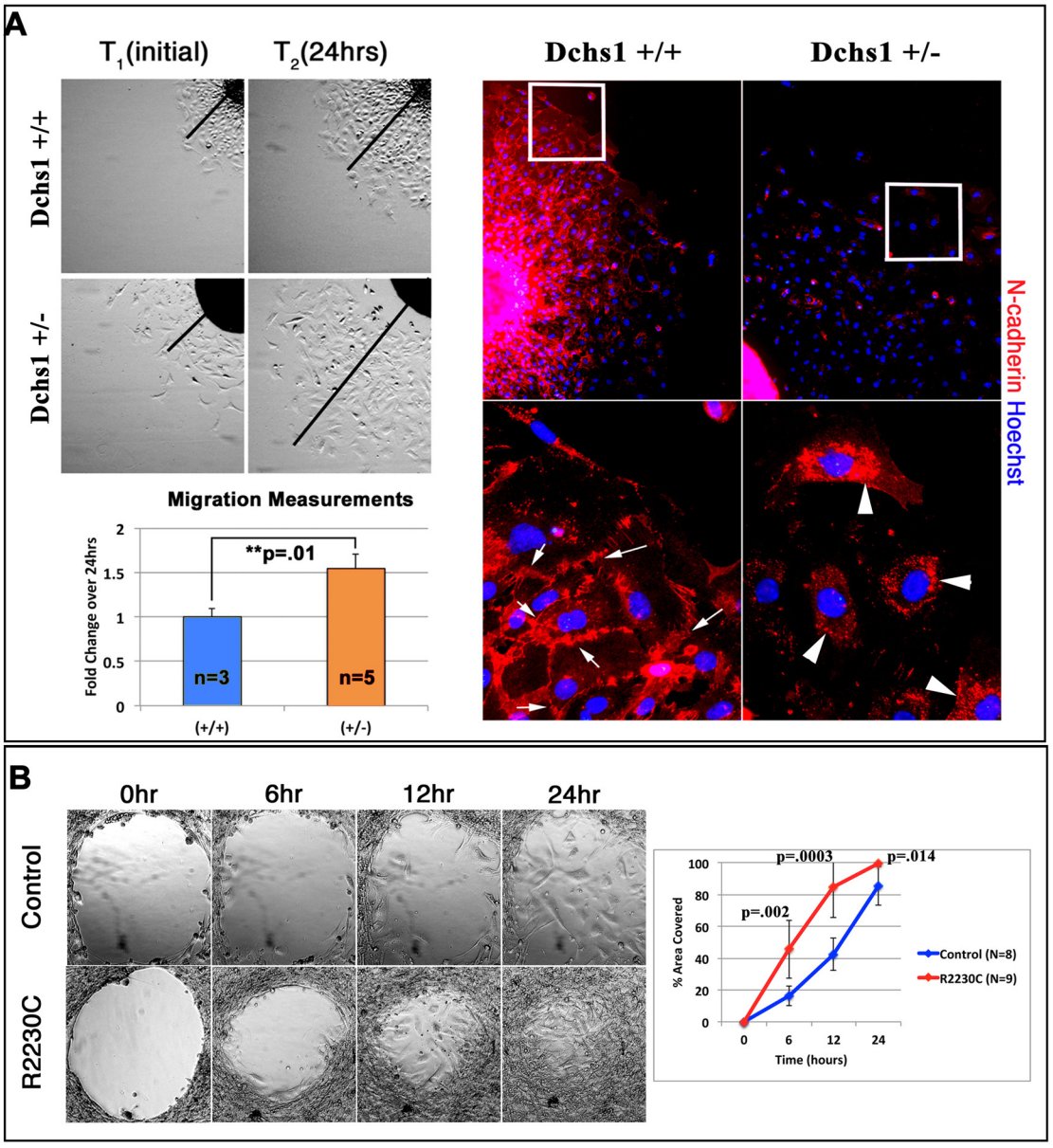

Extended Data Figure 10 | Mice and MVP patients with Dchs1 deficiency exhibit migratory defects *in vitro*. **a**, Posterior leaflets of P0 neonatal *Dchs1*$^{+/+}$ and *Dchs1*$^{+/-}$ mice were explanted and interstitial cells were allowed to migrate out for 24 h. *Dchs1*$^{+/-}$ mice exhibit increased migration (black lines drawn from explants) coincident with loss of cell–cell contacts and N-cadherin expression at focal adhesions. Whereas N-cadherin expression (red) is found at the membrane at points of cell–cell contract in *Dchs1*$^{+/+}$ valvular interstitial cells (arrows), this membrane expression is lost in the *Dchs1*$^{+/-}$ cells and is prominently expressed in the cytoplasm (arrows). Nuclei, blue. **b**, Migration assays using control and MVP patient (p.R2330C) valvular interstitial cells exhibit a similar affect as observed in the mouse cells whereby the p.R2330C cells exhibit an increase in migration. *P* values are indicated in graphs.